Space Sci Rev (2012) 173:223–245
DOI 10.1007/s11214-012-9888-y

Current Fragmentation and Particle Acceleration in Solar Flares

P.J. Cargill · L. Vlahos · G. Baumann · J.F. Drake · Å. Nordlund

Received: 3 February 2012 / Accepted: 27 April 2012 / Published online: 31 May 2012

Abstract Particle acceleration in solar flares remains an outstanding problem in plasma physics and space science. While the observed particle energies and timescales can perhaps be understood in terms of acceleration at a simple current sheet or turbulence site, the vast number of accelerated particles, and the fraction of flare energy in them, defies any simple explanation. The nature of energy storage and dissipation in the global coronal magnetic field is essential for understanding flare acceleration. Scenarios where the coronal field is stressed by complex photospheric motions lead to the formation of multiple current sheets, rather than the single monolithic current sheet proposed by some. The currents sheets in turn can fragment into multiple, smaller dissipation sites. MHD, kinetic and cellular automata models are used to demonstrate this feature. Particle acceleration in this environment thus involves interaction with many distributed accelerators. A series of examples demonstrate how acceleration works in such an environment. As required, acceleration is fast, and relativistic energies are readily attained. It is also shown that accelerated particles do indeed interact with multiple acceleration sites. Test particle models also demonstrate that a large number of particles can be accelerated, with a significant fraction of the flare energy associated with them. However, in the absence of feedback, and with limited numerical resolution, these results need to be viewed with caution. Particle in cell models can incorporate feed-

P.J. Cargill (✉)
Space and Atmospheric Physics, The Blackett Laboratory, Imperial College, London, SW7 2BW, UK
e-mail: p.cargill@imperial.ac.uk

P.J. Cargill
School of Mathematics and Statistics, University of St Andrews, St Andrews, Fife, KY16 9SS, UK

L. Vlahos
Department of Physics, Aristotle University of Thessaloniki, 54006, Thessaloniki, Greece

G. Baumann · Å. Nordlund
Niels Bohr Institute, University of Copenhagen, Juliane Maries Vej 30, 2100 Copenhagen, Denmark

J.F. Drake
Institute for Research in Electronics and Applied Physics, University of Maryland, College Park, MD 20742, USA

back and in one scenario suggest that acceleration can be limited by the energetic particles reaching the condition for firehose marginal stability. Contemporary issues such as footpoint particle acceleration are also discussed. It is also noted that the idea of a "standard flare model" is ill-conceived when the entire distribution of flare energies is considered.

Keywords Solar flares

1 Introduction

Understanding particle acceleration in solar flares remains a challenging problem. Background information can be found in many review papers (e.g. Miller et al. 1997; Benz 2008; Vlahos et al. 2009; Fletcher et al. 2011; Raymond et al. 2012). For many years evidence for the presence of energetic particles came from radiation at hard X-ray (HXR) and γ-ray (GR) wavelengths, while more recently imaging HXR and GR spectroscopy from the Reuven Ramaty High Energy Solar Spectroscopic Imager (RHESSI) mission has demonstrated the sites of the radiation. RHESSI results are discussed more fully in this volume by Raymond et al. (2012), but for completeness we note the following:

(i) Flares have energies in the range 10^{27}–a few 10^{32} ergs. Smaller discrete energy releases (e.g. nanoflares) are also postulated. Generally a "large" flare is considered to involve the release of about 10^{32} ergs.
(ii) HXR emission rises rapidly at the start of a flare (in seconds) and has very impulsive structure (sub-second), suggesting that the energy release is "explosive". The accelerated electrons form a power law above 10 keV, with energies attaining relativistic values. The shape of the distribution functions, and in particular the "soft-hard-soft" evolution of HXR spectra provides important information about the properties of the acceleration.
(iii) RHESSI data has shown that the predominant location of HXR emission are the (chromospheric) footpoints of closed magnetic field structures (coronal loops), though coronal HXR emission is also observed (Krucker et al. 2008).
(iv) Interpretation of footpoint HXR emission using the "thick target model" (TTM: Brown 1971; Brown et al. 2009) implies the acceleration in large flares of up to 10^{38} electrons to energies between 10 and 100 keV in a few hundred seconds.
(v) RHESSI has detected GR emission at loop footpoints associated with ions of energies 10–100 MeV, though not necessarily co-spatial with HXR emission (Lin et al. 2003; Emslie et al. 2004). The strong correlation between emission from >30 MeV protons and >0.3 MeV electrons (Shih et al. 2009) suggests a common acceleration mechanism. The number of energetic ions is less certain than electrons, but there is no reason why it cannot be large.
(vi) The soft X-ray (SXR) emission peaks some time (tens of seconds) after HXR emission. One can generically refer to the times when HXR (SXR) emission dominates as the impulsive (gradual) phase of a flare.

While both electrons and ions have long been known to be accelerated to relativistic energies, the flare "number and efficiency problems" have usually been framed in terms of sub-relativistic electron acceleration during the impulsive phase, in part due to the difficulty of detecting analogous evidence for sub-relativistic ions in and around the flaring region. We note that in the relativistic regime electrons and ions exhibit approximately proportional acceleration (Shih et al. 2009).

The focus on electrons is also due to the interpretation of HXR data using the TTM. Taking the requirement of 10^{38} accelerated electrons, and a flare volume of 10^{28} cm^3, then, for a typical pre-flare coronal density, at least the entire coronal population needs to be accelerated to energies in excess of 10 keV (the "number problem"). Further, for the measured HXR photon fluxes and distributions, the TTM implies that a very significant fraction (tens of %) of the total solar flare energy must be present in energetic electrons above 10 keV (the "efficiency problem"). Efforts to mitigate the former have been presented recently by Brown et al. (2009), as we will discuss more fully in Sect. 5. However, energetic ions are common in the solar wind after large flares and the correlation in emission from the most energetic electrons and protons noted above suggests that ion acceleration in flares is robust.

We summarize the requirements (in order of achievability) of the acceleration mechanism(s): acting on positively and negatively charged species, being fast, requiring particles to attain relativistic energies, perhaps involving a large fraction of the coronal population, and needing to be efficient. The first three are achievable using simple acceleration theories (e.g. a single shock, current sheet, turbulence etc.). The latter two seem to require a consideration of the global coronal magnetic field geometry, and the complexity inherent therein.

The source of the energy in the accelerated particles is the non-potential component of the coronal magnetic field, and the energy for flares of all energies and also the non-flaring corona is due to the conversion of the free energy in this field. However, the very weak coronal electrical resistivity makes dissipation difficult since, even with a substantial enhancement over a classical value, resistivity is only important on very small scales. Such small regions, generally referred to as current sheets, are the key building block in understanding energy release on all scales in the corona, and any study of particle acceleration needs to begin with how current sheets are formed and facilitate the release of magnetic energy (Sect. 2).

Once a current sheet (or multiple current sheets) form, and start to dissipate (or, in common parlance, to "reconnect"), the effectiveness of particle acceleration mechanisms both within the current sheets and in the region downstream where the reconnected field lines release their tension can be assessed (Sects. 3 and 4). Several examples of particle acceleration using test particle models in evolved magnetic fields, and also full particle in cell (PIC) codes, are presented. Flare acceleration by magnetohydrodynamic (MHD) and higher frequency turbulence is discussed elsewhere in this volume (Lazarian 2012; Petrosian 2012).

2 Current Sheets in Stressed Coronal Magnetic Fields

How current sheets form in the corona is a long-standing problem. The magnetic energy entering the corona is transmitted from (or through) the photosphere, either directly by the emergence of new magnetic flux, or via a Poynting flux associated with mass motions, which can be organized on a large scale, or be semi-random. It is now widely accepted that large-scale photospheric motions (which may also incorporate smaller scale semi-random components) leads to the formation of multiple coronal current sheets (e.g. Galsgaard and Nordlund 1996; Gudiksen and Nordlund 2005; Einaudi and Velli 1999; Rappazzo et al. 2010). The multiple current sheets form a hierarchy of scales that allows magnetic energy to be dissipated, no matter how small the dissipation scales are. On observationally resolved scales the distribution of the electric current must of course be consistent with the curl of the magnetic field on these scales, evolving only on the time scales on which

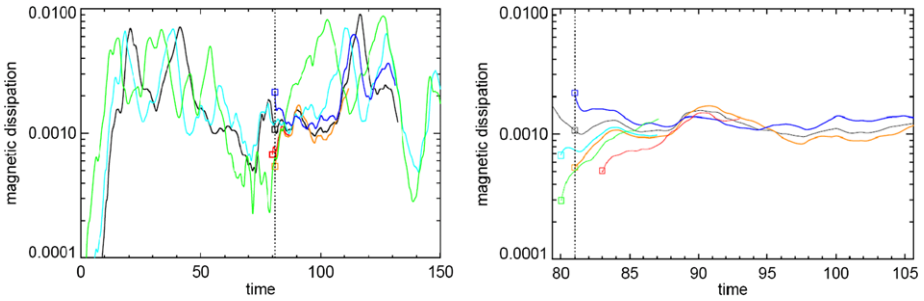

Fig. 1 The dissipation of magnetic energy in a braiding simulation as a function of time and numerical resolution. In the *left panel*, resolution increases from *green* ($128^2 \times 250$ cells), *pale blue* ($256^2 \times 500$), and *black* ($512^2 \times 1000$). In the *right panel*, three curves fork off the *black* one at $t = 81$. The *dark blue* one has $256^2 \times 500$ cells, having $512^2 \times 1000$ prior to $t = 81$, the *orange* one has $1024^2 \times 2000$ cells, again having $512^2 \times 1000$ earlier. In both panels, dissipation and time are in dimensionless units. From Nordlund and Galsgaard (2012). The dimensionless time is measured in units of Alfvén travel times, which are of the order of a few seconds for typical active region loop structures

the structures on these scales evolve; while on smaller scales the dissipation is correspondingly more intermittent in both space and time.

An example of such hierarchical current sheet formation comes from high resolution numerical simulations of "magnetic braiding" where the full resistive 3-D MHD equations are solved (Nordlund and Galsgaard 2012; a high resolution version of the experiment by Galsgaard and Nordlund 1996). These results should not be taken as representing how a large flare may proceed, rather to outline some important physical principles that apply to magnetic dissipation, which become apparent in such models. Nevertheless, as an aid in relating the non-dimensional time scales to real time scales; for typical coronal loop conditions time units (which are Alfvén travel times) are of the order of a few seconds.

The left panel of Fig. 1 shows dissipation as a function of time for three different numerical resolutions up to a maximum of $1024^2 \times 2000$ points, differing by consecutive factors of 2 (details in the figure caption). The right panel shows the reaction of the dissipation to restarting the runs at $t = 81$, where on restart the resolution is increased or decreased by a factor of two. When the resolution is doubled from $512^2 \times 1000$ to $1024^2 \times 2000$, the dissipation initially drops by about a factor of two, since the numerical resistivity scales with the mesh size. But shortly afterward the dissipation level returns to the previous level. Likewise, when the resolution is halved, the dissipation rises and then returns to its previous level.

The important feature is that over a long enough interval, there is a balance between the energy injected into the system by the driving at the boundary, and that being dissipated (e.g. Galsgaard and Nordlund 1996). This is NOT steady dissipation, since the magnitude of the dissipation changes by over an order of magnitude in a few time units (a few seconds). The energy input scales with the driving speed and magnetic energy density as well as the angle that field lines make with the driving boundary. In turn, this angle is determined by the "winding number", namely the fact that the coronal magnetic field lines cannot be wound up by more than about one turn between the two photospheric boundaries. Any attempt to increase further the angle at the boundary results in kink-like instabilities which in turn reduce the average twist by creating smaller scale dissipative structures ("hierarchical dissipation"). Hence, when boundary driving is continuous, the angle will remain at a semi-stationary level (marginal stability), and so will the work done on the plasma, and by implication the dissipation level.

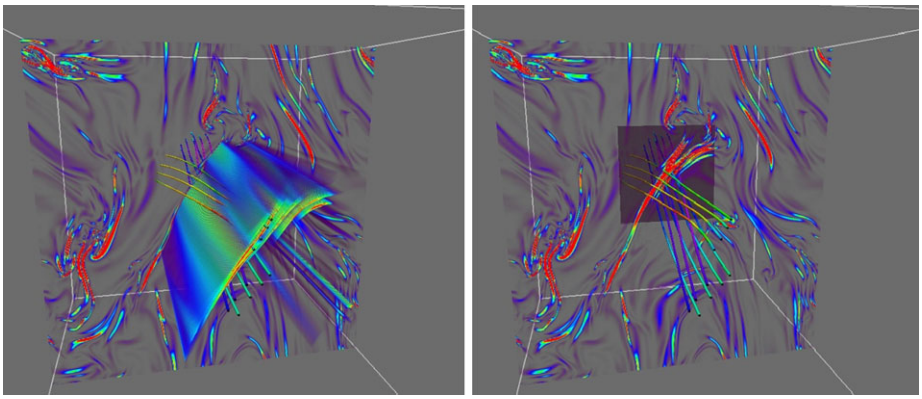

Fig. 2 Sample results of a high-resolution ($1024^2 \times 2000$) 3-D braiding simulation. The *left panel* shows the current structure, with the central current sheet emphasized. This is in a state of the beginning of fragmentation. Several smaller, secondary current sheets are also visible, stacked on top of each other behind the large current sheet. In the *right panel*, the central current sheet has been removed, revealing the central plane cross section (enhanced with a *dark square*), where the *color image* shows the magnitude of the electric current density. The current sheet fragments cutting through that plane are outlined with sets of magnetic field lines, manually placed between the current sheet fragments. From Nordlund and Galsgaard (2012)

Figure 2 shows the current structure in a high resolution ($1024^2 \times 2000$) simulation. The left and right panels show, respectively, the fragmentation of the large central current sheet, with subsidiary current sheets surrounding it. On the left, not only can very filamentary current structure be seen throughout the simulation box, but the large central current sheet is itself beginning to fragment. On the right, the central current sheet has been artificially removed to reveal the field structure there. Three sets of field lines have been placed between the current sheet fragments. The fragmentation occurs because, at some distance along the field lines, the three sets of field lines connect to fluid moving in different directions. This results in an increasing difference in orientation between the sets of field lines, which causes the current sheet fragments to appear and grow in strength. The fragmentation may be expected to continue, recursively, resulting in a hierarchical structure of current sheets, with scales extending down to physical scales where resistive diffusion is sufficiently important to prevent further fragmentation. The experiment in Fig. 2 was performed in dimensionless units, but one can imagine this kind of hierarchical structure in the solar corona ranging from an outer scale of order Mm down to dissipation scales many orders of magnitude smaller.

A common misconception about numerical MHD experiments can also be addressed with such high resolution experiments. Computational resistivity models (which can be either explicit or implicit in the numerical method—the one used here is described in Baumann et al. 2012a) put resistivity where it is needed (e.g. to ensure that current sheets remain resolved with a few mesh points) and minimizes it where smaller values are sufficient. This is done to increase the effective numerical resolution for a given mesh size. However, as can easily be demonstrated with current computational capacities, similar results are obtainable using constant resistivity and a larger number of mesh points, just at correspondingly higher computational cost.

An alternative approach to coronal current sheet formation began with the work of Lu and Hamilton (1991). They used ideas from self-organized criticality (SOC: Bak 1999) to show that when the coronal magnetic field was driven continually and randomly, and subjected to rules about relaxation to a lower energy state, dissipation occurred in temporally discrete

events with a wide range of energies. The event sizes formed a power law, roughly E^{-b} with b between 1.5 and 1.9, similar to that associated with flares over a wide energy range (e.g. Hudson 1978; Crosby et al. 1993; Aschwanden et al. 1998; Miroshnichenko et al. 2001). It is remarkable that such a simple model gave this result, especially since it suffered from a number of flaws, including there being no guarantee that Faraday's law was satisfied. However, a subsequent body of work (e.g. Vlahos et al. 1995; Vassiliadis et al. 1998; Isliker et al. 2001; Charbonneau et al. 2001) removed these inconsistencies while retaining power law distributions of flare energy.

Indeed, such SOC/Cellular automata (CA) models can include quite general photospheric drivers including emerging flux. In a series of recent studies (Vlahos and Georgoulis 2004a; Dimitropoulou et al. 2009, 2011) an active region was modeled using linear or nonlinear extrapolation of a photospheric magnetogram. Small-scale structures (current sheets) formed readily. It was then assumed that all discontinuities which reached a specific threshold relaxed, and redistributed the free energy to their neighbors, causing primary and secondary bursts. When the system was completely relaxed, a new magnetic increment was added randomly inside the active region, so continually "loading" the active region with magnetic energy, similar to the approach of Lu and Hamilton.

An example of this is shown in Fig. 3. The two panels in the left column show the magnetic field lines in two active regions. The upper right panel shows the location of discontinuities that exceed various thresholds for dissipation and the lower right one maps the discontinuities to the photosphere. It can be seen that such driving leads to the formation of many flaring regions in the volume, with sizes and energetics in close agreement with observed flare statistics. It must be emphasized that the key feature of SOC-based models is that the flare takes place at multiple locations, with particle acceleration presumably going on at all of them. Comparison of these results with the observed distribution of flares above specific active regions is underway (Dimitropoulou et al., private communication).

The connection between SOC and self-consistent MHD models has yet to be established rigorously, though it should be noted that some MHD models of a turbulent corona do give rise to many of the power law distributions in event size, waiting time etc. (e.g. Galsgaard and Nordlund 1996; Buchlin and Velli 2007; Rappazzo et al. 2010). However, while SOC models are quick to run for long times with large systems, ultimately solutions of the full MHD equations are desirable to establish the state of the coronal field in response to a photospheric driver. In addition, it is highly desirable that a proper comparison of an identical problem with SOC and 3D MHD be undertaken.

While the above developments indicate the complex magnetic nature of the flaring corona, more traditional flare models relying on a single current persist and indeed are sometimes referred to as the "standard model" (Shibata 1998; Shibata and Magara 2011). The basis of this lies in a scenario for large eruptive flares as the outcome of the shearing of the coronal magnetic field by oppositely-directed photospheric motions on either side of a neutral line (e.g. Sturrock 1966; Kopp and Pneuman 1976). As the free energy in the corona builds up, the magnetic field becomes unstable, or loses equilibrium, and erupts, ejecting material (often a prominence) into interplanetary space. Because of their size, such large flares (often called two-ribbon flares) are studied extensively.

It is argued that the eruption (or ejection) plays a central role in establishing a single laminar extended coronal current sheet, with the eruption driving the entire flare. [This contrasts with Kopp and Pneuman (1976; see also Cargill and Priest 1982) who invoked the coronal current sheet to account only for so-called "post-flare loops" in eruptive flares.] The SOC-class of models do not as yet account for such large-scale mass ejections, and consequently they do not rely on such eruptions to drive other aspects of the flare. Thus, although

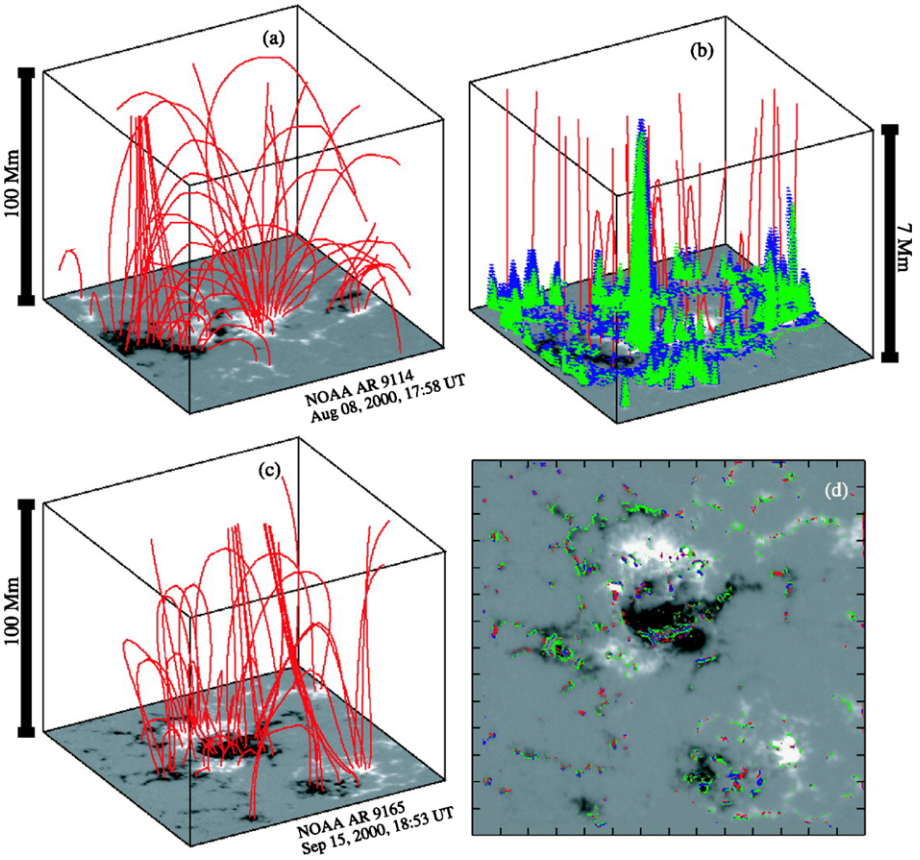

Fig. 3 Force-free magnetic field modeling of an active region. The *upper left panel* shows the linear force-free field (*red*) in NOAA AR 9114 and *upper right* shows the lower part of the active-region atmosphere, as indicated on the vertical axis. Shown are magnetic field lines (*red*), with the identified magnetic discontinuities for a "Parker angle" $\Delta\theta = 10°$ (*green*) and $\Delta\theta = 8°$ (*blue*). The *lower left panel* shows the linear force-free field in NOAA AR 9165 and in the *lower right* is a projection of the detected magnetic discontinuities at the photosphere (*green*) (Vlahos and Georgoulis 2004a)

eruptions clearly do happen in large flares, they are likely to be one part of the generic flare process rather than the central essential feature, as is argued in the "standard model".

However, there seems no reason why the elongated current sheet in such models cannot fragment, as shown in Fig. 2. Indeed, recent kinetic models of reconnection with an ambient guide field indicate that secondary islands or flux ropes form spontaneously and grow to finite size (Drake et al. 2006b; Daughton et al. 2011) and such kinetic models also call into question the traditional single x-line model of flares. Similar considerations apply to coronal current sheet formation where the pre-existing coronal field interacts with the emerging field (e.g. Heyvaerts et al. 1977), and leads to a flare and/or eruption. Numerical models of flux emergence suggest that such current sheets can fragment, leading to a rather complex environment (e.g. Hood et al. 2012).

3 Properties of Dissipation Sites and the Formation of Accelerators

The current sheets discussed in Sect. 2 have a scale (especially width) determined by the resolution of the model. So, for a $1024^2 \times 2000$ MHD simulation with a uniform grid, the minimum scale that can be resolved is $2/1024 = 1/512$ length units. Since the global scale determines the unit of length, and if we assume this is 10^9 cm, then current sheets of width 20 km are "resolved". With adaptive rezoning this number can be improved, though such a process is difficult in a model with multiple current sheets. As discussed above, a hierarchy of current sheets is expected to develop in systems with smaller resistivity, but numerical models will never be able to reach the full range of scales expected to occur in the solar corona. What then has the dissipation level in current sheets with width 20 km got to do with the real corona where predictions of current sheet width based on classical transport or non-MHD physics are orders of magnitude less?

The main answer comes from the work/dissipation balance argument of Galsgaard and Nordlund (1996), as discussed further in Baumann et al. (2012a). Figure 1 showed that the magnetic energy fed into the current sheets ends up being dissipated irrespective of the resistivity, or numerical resolution, and hence the current sheet width, even over times scales so short that no growth or reduction of hierarchical structure has time to occur. The explanation is that, even within the same current sheet structure, a simple scaling of the current sheet thickness leads to a quick recovery of the dissipation level. The process may be illustrated by considering the effect of resistivity scaling in numerical experiments.

The ultimate purpose of resistivity in numerical experiments is to prevent current sheets from becoming unresolved. The actual form can vary, from uniform in space to non-uniform, with larger values in current sheets than outside. Nevertheless, the overall magnitude must scale with the mesh size, in order to adjust to varying numerical resolutions. The consequence, and indeed the purpose of the scaling, is to keep current sheets resolved, independent of what the cell size happens to be. Thus, for a given jump of magnetic field direction across a current sheet of width Δs, the values of the current density J, resistivity (magnetic diffusivity), and Joule dissipation Q scale as $J \sim \Delta B/\Delta s$, $\Delta s \sim \eta$ and $Q \sim \eta J^2 \sim 1/\Delta s$ respectively. But since the area where the dissipation Q occurs scales as $A \sim L\Delta s$, where L is the current sheet length (in the direction perpendicular to the current), the total dissipation per unit length along the electric current direction scales as AQ, independent of resolution. This also implies that the resistive electric field, ηJ, is independent of the current sheet thickness and of order $U\Delta B$ where U is a typical driving velocity of the system. This simple scaling only applies as long as the motion patterns necessary to transport mass and (in particular) guiding field can be accommodated (i.e. the maximum velocities required do not exceed the Alfven speed). Further reductions of current sheet thickness require additional fragmentation, which reduces also the "width" of the current sheet fragments, thus alleviating requirements on flow speeds.

While this suggests that some confidence can be placed in MHD models, and in Sect. 4 we discuss a number of such models where particle acceleration is considered within a global magnetic field framework, fundamental issues remain. Specifically, it has been argued that MHD models overestimate the real thickness of current layers. One of the results of Hall reconnection models is to demonstrate that the current layers contract sufficiently compared with the MHD description to explain the fast rates of release of magnetic energy seen in nature (Karimabadi et al. 2007; Shay et al. 2007). For example, reconnection encounters in the solar wind reveal few current layers per se, but do show reconnection exhausts associated with the presence of current layers that scale to more than 10^6 km. This question of which scale various processes occur on (global MHD, current dissipation and particle acceleration

scales are all going to be different), is one of the major obstacles standing in the way of a complete theory of flares and raises many questions. Examples include whether current layers versus Petschek-like slow shocks operate as a flare heating mechanisms (Longcope et al. 2010) and the fact that different species may be heated and different particles accelerated depending on the current sheet scales (Drake et al. 2009; Knizhnik et al. 2011).

Current sheets (or reconnection sites) have three potential generic accelerators: shocks, turbulence (MHD or higher frequency) and DC electric fields. The first, while very effective in the solar wind, at planetary bow shocks and for other astrophysical scenarios, has difficulties in the strong magnetic field of the corona. For a shock to form, flows in excess of the fast mode magnetosonic speed are required and for flares, plasma jets of order $>10^3$ km/s are required. There are though some caveats to this conclusion. Slow mode shocks are a central part of many reconnection models (Petschek 1964; Longcope et al. 2010) and require flows of order the sound speed to form. However, while they can heat plasma effectively (Cargill and Priest 1982), they are not effective as accelerators (Isenberg 1986; Kundu et al. 1989). Secondly, fast mode termination shocks may arise when reconnection-produced flows run into neighboring magnetic field lines. Observational evidence for outflows strong enough to produce such a shock is weak, but that does not rule out their presence in local, sub-resolution reconnection sites. However, these will be quasi-perpendicular shocks, and so are not terribly efficient as an accelerator of large numbers of particles, through ripples in the shock front could mitigate this. Thirdly, the 3-D coronal field can possess many null points (Maclean et al. 2009), which act as dissipation sites, and could encourage more ready shock formation due to the weak local field.

It is argued that MHD turbulence can arise from the evolution of plasma flows (jets) generated at reconnection sites through a standard "eddy turnover" argument in which a jet degrades into a spectrum of fluctuations. However, there are some concerns. The magnetic field profile in a plasma jet will have a predominant component along the current sheet (the guide field). This will advect passively as any jet degradation takes place (there is no associated tension force). On the other hand, the planar magnetic field exiting the current sheet will resist the jet degrading due to a magnetic tension force. So far as we are aware, there are no calculations one way or the other on this question which certainly merits investigation. An alternative approach is to argue that flare energy release is such a dramatic process that a spectrum of fluctuations can always be generated.

Further issues with turbulence in flares are the following. Because of the high efficiency of acceleration, it would seem to be required that there is a very efficient energy conversion process (a) from the jet to the turbulence, and (b) from the turbulence to the particles and, as a consequence, (c) any turbulence present needs to be "strong" in the sense that the usual assumptions (quasi-linear etc.) are unlikely to be relevant (see Cargill 1996 and Miller et al. 1997 for a further discussion). On the other hand, the "injection problem" associated with MHD turbulence was addressed by Miller and Roberts (1995) and Miller et al. (1996) who demonstrated how both electrons and ions could be accelerated from a thermal population by fast mode and Alfven waves respectively. Turbulent (or stochastic) acceleration is discussed in more depth in this volume by Lazarian (2012) and Petrosian (2012).

The theory of particle motion and acceleration in a single laminar current sheet has a long history (e.g. Speiser 1965; Chen 1992), and has been studied in the corona (e.g. Martens and Young 1988; Oreshina and Somov 2006; Dalla and Browning 2006) who demonstrated the need to include all magnetic field components in the calculations. However, while this test particle approach is useful, in recent years the study of particle acceleration in current sheets has moved in other directions, as developed in the next Section. Important developments have been the recognition that elongated current sheets tend to break up (or fragment) into

multiple regions of intense current, as shown in Fig. 2 so that particle acceleration is now no longer limited to a single "monolithic" current sheet, as in the "standard model". Also, the work on the Hall reconnection model in collisionless (Birn et al. 2001; Shay et al. 2007; Karimabadi et al. 2007) and weakly collisional (Cassak et al. 2005) current sheets has provided a firm underpinning of this important regime and now provides a starting framework for understanding the acceleration of particles during collisionless reconnection.

4 Acceleration by Direct Electric Fields in Current Sheets

Having established the context of particle accelerators in a global magnetic field, we now turn to the actual acceleration processes operating in current sheets. Several examples are shown using a range of techniques ranging from test particles in MHD models to full particle in cell (PIC) simulations.

4.1 Acceleration in Fragmented Current Sheets

We first show results due to Onofri et al. (2006) of current sheet fragmentation accompanied by particle acceleration. [Other simple examples can be found in Dmitruk et al. (2003).] A single field reversal with a superposed guide field is set up, and allowed to evolve using a 3-D MHD code. The nonlinear evolution is shown in the three left panels of Fig. 4 and is characterized by the formation of small scale structures on either side of the initial current sheet, and coalescence of magnetic islands in the center. Ultimately, the initial current sheet is entirely destroyed, the narrow, confined current sheet broadens into a large-scale region of turbulence, and the electric field becomes highly fragmented. Acceleration can occur at the strong electric field regions and the distribution of these regions in space fills a large portion of the simulation box at later times. The magnitudes of the electric field are well in excess of the Dreicer field. The right panel of Fig. 4 shows the outcome of injecting electrons as test particles into a snapshot of the evolved fields. There is very fast (100 μs), effective acceleration of the electrons, with a tail being formed up to relativistic energies. Injecting protons gives a more limited, slower (ms), acceleration with energies of up to 1 MeV. Note that these timescales are very short, suggesting that measured impulsive phase rise times have less to do with the actual acceleration physics as opposed to the global field dynamics.

An important point is that the particle energy gain in these test particle simulations rapidly exceeds the available free energy in the magnetic field. One effect of this is that ion acceleration would be very limited because the electrons acquire most of the available free energy in the system. In addition, there needs to be a process that, as energy goes from the magnetic field to the particles, limits and eventually terminates the acceleration. Such "feedback" of the energetic particles on the field is a recurrent theme in this section.

The results of PIC simulations also support the basic picture of reconnection occurring at multiple sites in 3-D (Drake et al. 2006a; Daughton et al. 2011). However, carrying out 3-D simulations with sufficient separation of scales to explore how particles interact with multiple reconnection sites and associated magnetic islands, remains beyond the capability of the largest available computing platforms. Instead, a useful model has been a 2-D multi current layer system. Figure 5 shows the out-of-plane electron current at three times during the evolution of a system with an initial state of 16 current layers and an ambient guide field that is half the strength of the reversed magnetic fields, except within the current layers where the guide field is increased to provide pressure balance. The initial plasma density is uniform and electron and ion temperatures equal. Magnetic islands grow from noise in

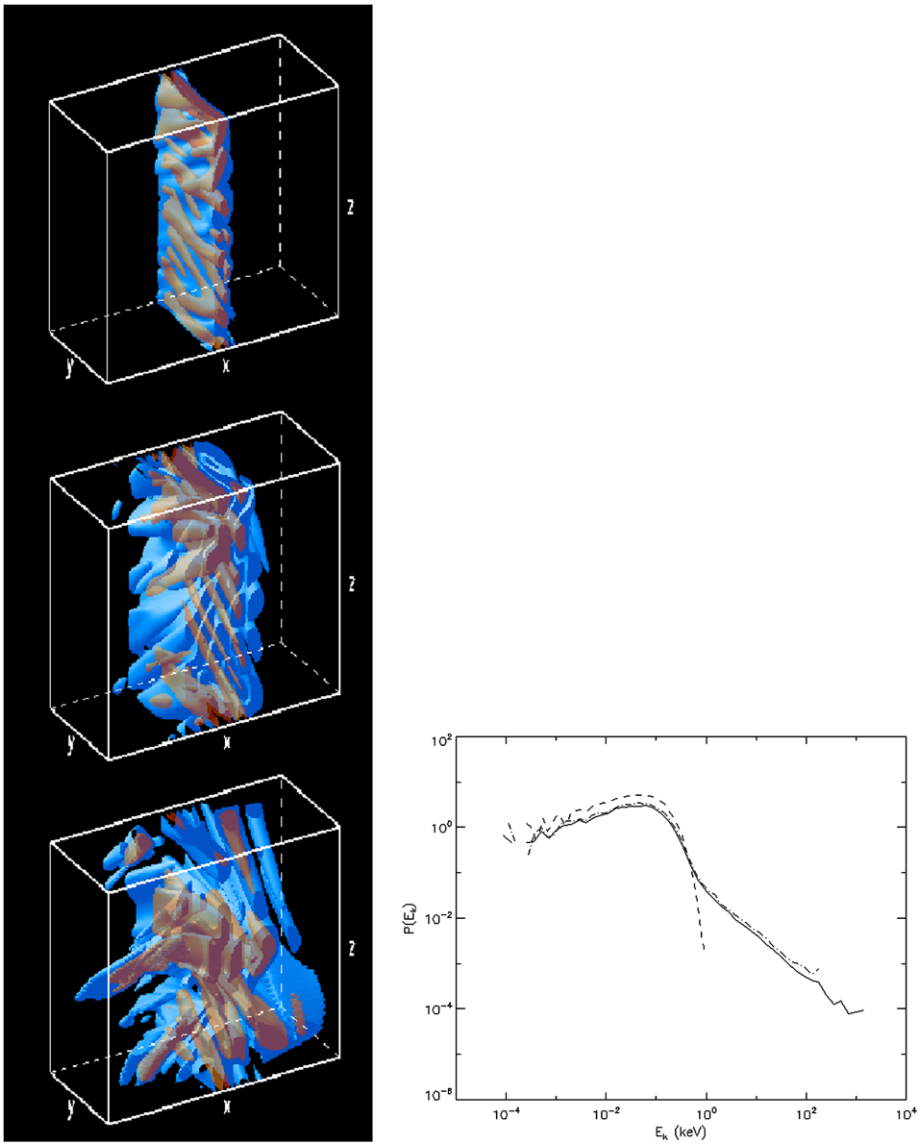

Fig. 4 The *left column* shows electric field isosurfaces at $t = 50$, $t = 200$ and $t = 400$ in a 3-D resistive MHD simulation of a fragmenting current sheet. Time is measured in units of an Alfven transit time. The *right column* shows the distribution function of electron kinetic energy obtained from running test particles through the electric and magnetic fields in the fully evolved current sheet ($t = 400$). The *dashed*, *dash-dotted* and *solid* lines show the distribution at $t = 0$, 3×10^{-5} and 8×10^{-5} secs respectively (from Onofri et al. 2006)

each current layer and quickly start merging with islands on the same layer. Island growth and merging continues until islands on adjacent current layers start merging. At late times the system has evolved into a sea of magnetic islands with little evidence of the original structure. It is evident from this behavior that both electrons and ions interact with many

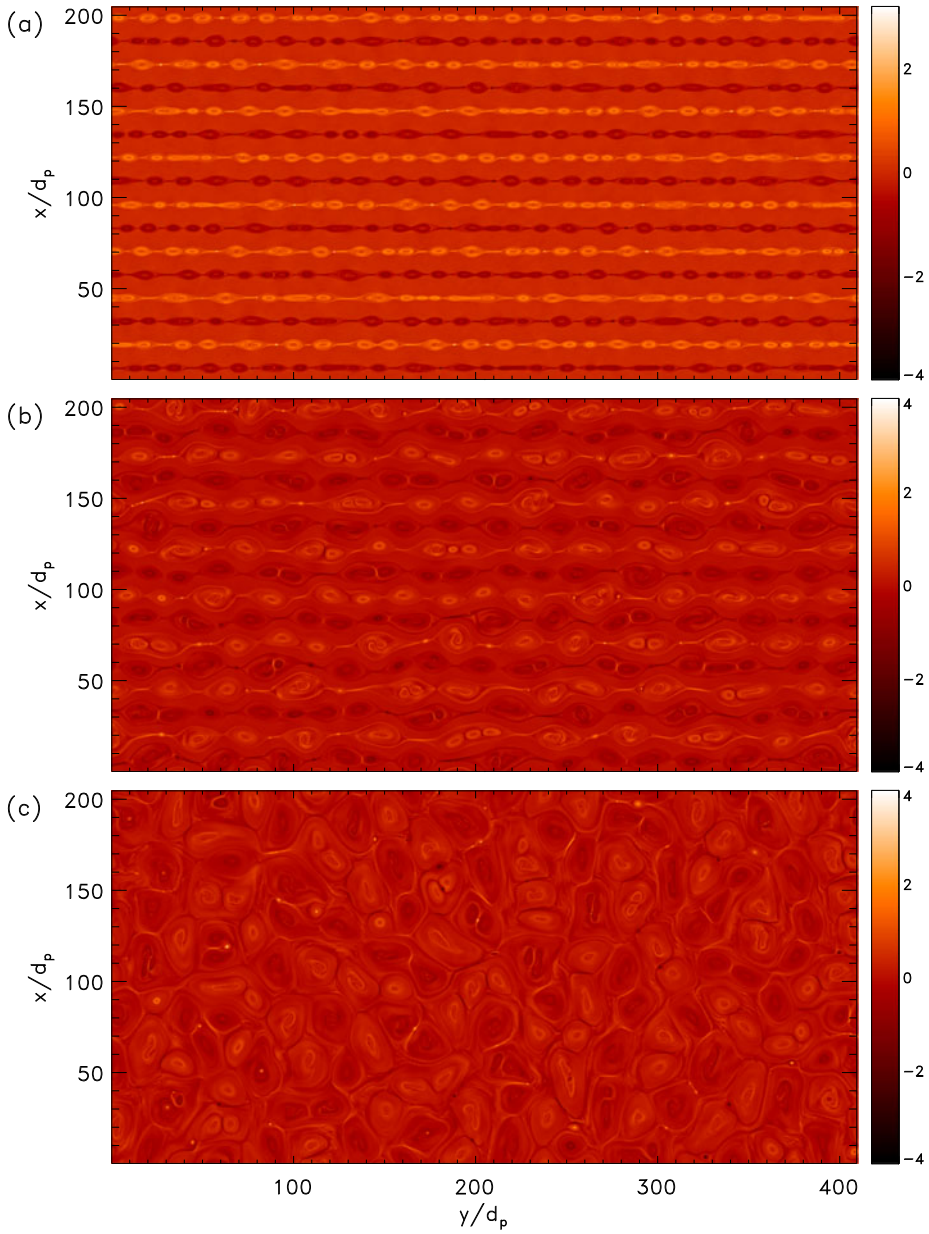

Fig. 5 The spatial distribution of the out-of-plane electron current at $t = 50, 100$ and 150 during the evolution of a PIC simulation of a multi current-layer system with an ambient guide field strength that is half of the reconnecting magnetic field. Time is in units of the inverse proton cyclotron frequency based on the reconnecting field and the spatial scale is in units of the proton inertial length

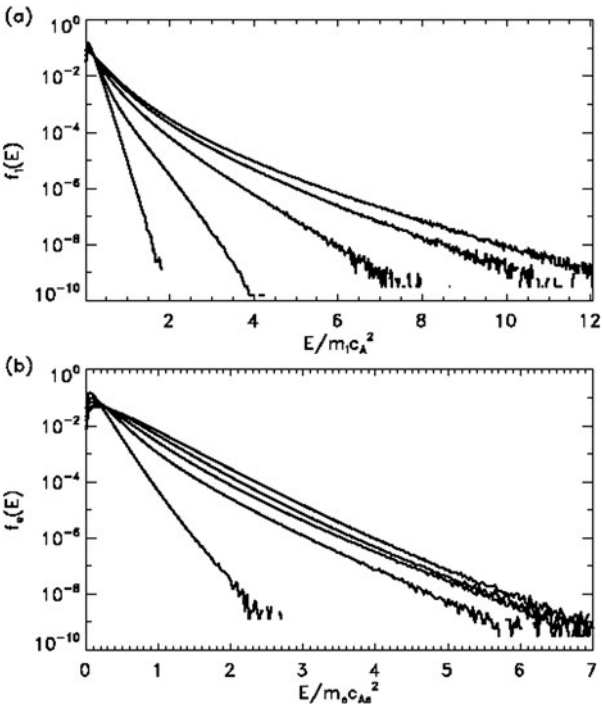

Fig. 6 The energy spectra of ions and electrons from the simulation of multiple current sheets shown in Fig. 5 at $t = 0, 50, 100, 150$ and 200 with the time increasing with the curves from left to right. Note that the plot is on a log-linear scale

magnetic islands as the system evolves, even though in a 2-D system the field lines are not stochastic.

Figure 6 shows the energy spectra of ions and electrons from the entire simulation domain at five times. Note that the energy increment of particles is roughly proportional to energy (the figure has a log-linear scale). This suggests that the acceleration mechanism of both species is a Fermi process in which the rate of energy gain of a particle is proportional to its energy. In earlier simulations without a guide field (Drake et al. 2010; Oka et al. 2010; Schoeffler et al. 2011) it was shown that the dominant mechanism for particle energy gain was through the Fermi reflection of particles circulating in contracting and merging magnetic islands. Particles gain parallel energy as they reflect from the ends of the islands, which are moving inward at velocities of the order of the Alfven speed based on the reconnecting magnetic field:

$$\frac{d\varepsilon_{||}}{dt} = 2\varepsilon_{||}\frac{v_x}{L}\frac{B_x^2}{B^2},$$

where v_x is the contraction velocity and L is the length of the island.

A surprise in Fig. 6 is the apparent abrupt drop in the rate of electron energy gain early in the simulation while during the same period the ions continue to gain energy. This behavior was not seen in the earlier simulations with anti-parallel magnetic fields and at the present time is not understood. In a simple model in which reconnection and the Fermi mechanism is suppressed by the approach to the marginal firehose condition (see Sect. 4.6) it was shown that the electron and ion energy spectra are power laws with a spectral index that takes the limiting value of 1.5 in the limit of a plasma with very low initial beta.

The recent over-the-limb observations by the RHESSI spacecraft (Krucker et al. 2010) are consistent with several features of this model. First, all of the electrons in the flaring

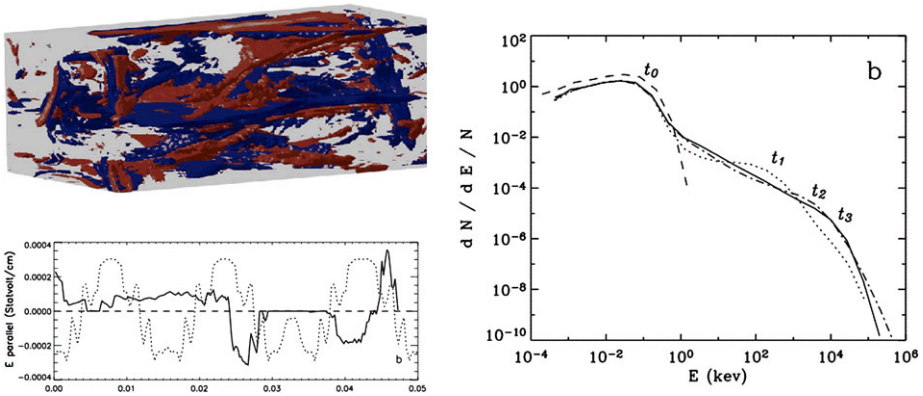

Fig. 7 Particle acceleration in a braided, fragmented coronal field (Turkmani et al. 2006). The *upper left panel* shows the resistive electric fields, frozen at a given time. The *lower left panel* shows the electric field experienced by a trapped (*dashed*) and untrapped particle (*solid*) as a function of time (dimensionless units). Note the different intervals of energy gain and loss. The *right panel* shows the energy spectrum at four different times

region high in the corona are part of the energetic component. Thus, all electrons undergo acceleration as expected since all electrons within an island are accelerated. Second, the total pressure of the energetic electron spectrum is of the order of that of the magnetic field, a prediction of the model.

4.2 Global Braided Magnetic Field

Turkmani et al. (2005, 2006) and Cargill et al. (2006) discussed particle acceleration in a stressed magnetic field. The approach is an earlier version of that discussed in Sect. 2 and involved starting with straight magnetic field lines connected to the photosphere at either end. Photospheric motions drove a Poynting flux into the corona, leading initially to the generation of global currents. After some time, these currents began to concentrate into local current sheets which then dissipated. The MHD aspects have been well understood for some time (e.g. Galsgaard 2002). The magnetic and electric fields were then frozen at a given time, and test particles run through the fields. The resistive electric field at a given time is shown in the left panel of Fig. 7, and its fragmented nature is evident. For this case, a short loop (20 Mm length) was used.

For an initial distribution with temperature of 5 MK, both electrons and protons were accelerated effectively through multiple interactions with the electric field, as shown in the lower left panel in Fig. 7. The particles move through different current sheets, gaining (and occasionally losing) energy at each one. Energies well in excess of 100 keV with hard spectra are obtained for both electrons and protons, with the protons taking about 10 times longer to become accelerated. The right panel of Fig. 7 shows a typical distribution function.

The hard spectra here give rise to a significant problem, namely the embarrassing efficiency of the process, with the energy in the test particles exceeding that available in the magnetic field. One can draw similar conclusions to the previous section, namely that the species that is accelerated faster will get all the available energy, and some sort of feedback is essential. Feedback will certainly limit the maximum energy, giving softer spectra, but the details are not known at this time.

However, numerical effects may also play a role in these large efficiencies. Such older results use quite coarse numerical resolution for the MHD model. As noted in Sect. 3, the

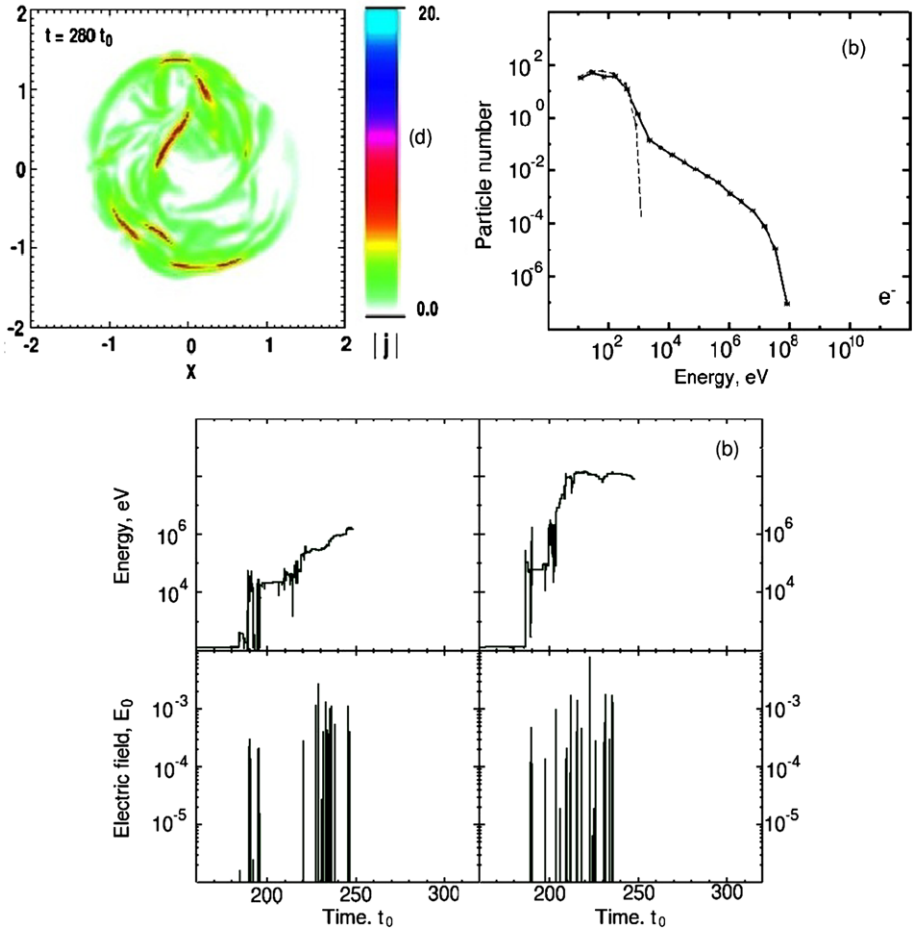

Fig. 8 Particle acceleration in a kink unstable loop. The *upper left panel* shows surfaces of iso-current as the instability enters its most turbulent phase. Space and time are both in dimensionless units, but typical coronal scales may be readily substituted. The *lower panel* shows (*upper*) the energy of typical electrons and (*lower*) the electric field magnitude experienced by the particle as a function of time. The *upper right panel* shows the distribution function of an ensemble of electrons after encountering the fragmented currents. From Gordovskyy and Browning (2011)

electric fields are of order *UB*. The resistive field is the most important one for particle acceleration, and will operate over the width of any current sheet. With 100^2 cells in the direction transverse to the guide field, and current sheets typically spread out over 3 or 4 cells, the current sheet cross-section is large, and indeed the current sheets are occupying a considerable (and probably unrealistic) fraction of the grid. Such an electric field acting over a numerically broadened and lengthened current sheet will interact with, and so accelerate, more particles than in a "real" (or better resolved) current sheet.

4.3 Kink Unstable Coronal Loop

What can be achieved with better numerical resolution is described in Gordovskyy and Browning (2011). Earlier work (Browning et al. 2008; Hood et al. 2009) has used high reso-

lution MHD simulations to study the non-linear evolution of the kink instability. A cylindrical twisted magnetic field is embedded within a potential field and the twist increased until the kink instability threshold is reached. The non-linear evolution of the instability involves the formation and dissipation of a single current sheet into a highly turbulent state (Fig. 8, upper left panel). Initial analysis suggests a k^{-2} scaling of these structures (Hood et al. 2012, private communication), but measurements are only possible over roughly a decade due to the numerical resolution. Eventually, the twisted field relaxes into a marginally stable state, as discussed in Sect. 2. In reality the process would recur if continual twisting was provided, leading to repeated dissipation and relaxation around marginal stability.

Gordovskyy and Browning (2011) have studied particle acceleration during the non-linear phase of the instability. Using test particles, they studied the acceleration of both electrons and protons. The overall features are similar to those found by Turkmani et al., namely acceleration of particles well in excess of 100 keV through multiple interactions with electric fields (Fig. 8, lower panels). However, the spectra are softer than found by Turkmani et al. (Fig. 8, upper right). Also, Gordovskyy (2011, private communication) has noted that the efficiency of the acceleration is about 5 %, a level where the feedback of the energetic particles on the field is not an issue.

Why do these two models have different efficiencies? There are two possible reasons. One is that the kink instability model has quite a small energy release, with 1–2 % of the available magnetic energy being dissipated. This is characteristic of the evolution of a system around a state of marginal stability, as is occurring here. The second possible reason for the reduced efficiency lies in the numerical resolution. The resolution in Gordovskyy and Browning (2011) is a factor of 5 better than in Turkmani et al., implying that the "cross-section" of the current sheets is a factor 25 less, making it less likely that the test particles encounter the current sheets.

4.4 Distributed Accelerators in SOC Models

We now address acceleration in an environment of many nonlinear acceleration sites such as arise from the SOC models discussed in Sect. 2. The outcome is an acceleration environment which has the characteristics of a more complex "accelerator" with distributed strong electric fields. Early work by Arzner and Vlahos (2004) considered collisionless test particles in evolved homogeneous turbulence using concepts borrowed from CA models. This new environment is born out of more complex statistical properties, which are not related to the standard Fokker Planck equation arising from weak turbulence.

Vlahos et al. (2004b) studied such complex environment, originating also from the CA models. Their main assumption is that the fragmentation of the energy release [either starting from the complexity arising from CA models, or from the work of Turkmani et al. (2006) or Gordovskyy and Browning (2011)] will lead to (in the statistical sense) the same generic accelerator, where the local accelerators are distributed inside the active flaring volume and particles are energized by visiting the localized and intermittent accelerators. The end result is a very special type of turbulent environment with "nodes" of accelerators distributed inside the energy release volume, as shown in the left panel of Fig. 9. Using Monte Carlo techniques and assuming that test particles follow a probability distribution for jumping along the nodes, and the energy gain before leaving the node, they obtain the kinetic energy distributions shown in the right panel of Fig. 9. Using Gaussian distributions for the above distribution give the standard Fokker Planck distribution and Fermi acceleration. If the probability distributions for the spatial diffusion and energy diffusion are power laws, an "anomalous first order Fermi-like" accelerator is naturally generated by the SOC type

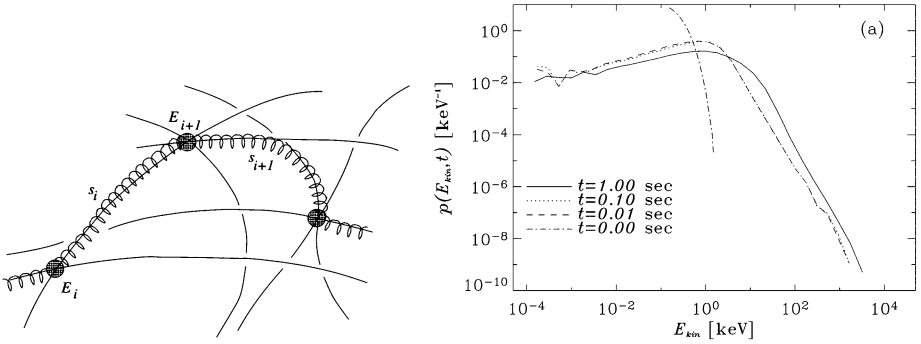

Fig. 9 The *left panel* shows a sketch of the basic elements of model discussed in Sect. 4.4: a particle (the *spiral line*) follows basically the magnetic field lines (*solid*), although also undergoing drifts, and travels in this way freely a distance s_i until it enters a current sheet (*filled circles*), where it is accelerated by the associated effective DC electric field E_{i+1}. After the acceleration event, the particle again moves freely until it meets a new current sheet. The *right panel* shows the kinetic energy distributions for the electrons using Monte Carlo techniques and assuming reasonable probabilities for the s_i and E_i (Vlahos et al. 2004b)

theories but also arising in recent multi-island type simulations. The lack of feedback on the formation of this environment is again apparent. The anomalous first order Fermi like accelerator follows a fractional diffusion equation (Bian and Browning 2008).

4.5 A Cross-scale Coupling Experiment Using a PIC Code

As noted above, the importance of the coupling of micro and macro scales lies at the heart of understanding flare particle acceleration. An interesting new development in this direction has very recently been taken by Baumann et al. (2012a, 2012b). Starting out from a potential field extrapolation of a SOHO MDI magnetogram of the active region on November 16th, 2002, which resulted in a fan-spine geometry with a null point located in the lower corona, a stretched-grid MHD simulation with a minimum cell size of 80 km and a constant density and temperature was conducted on a total region of $175 \times 100 \times 62$ Mm. The system was driven from the bottom boundary of the computational box, simulating the observed horizontal motion of the magnetic fragments, caused by flux emergence. This motion introduced a shear in the relative orientation of the magnetic field lines of two different connectivity domains separated by the fan-plane, which then gave rise to a strong current sheet and a resistive electric field in this region (for details see Baumann et al. 2012a).

After reconnection in the vicinity of the null point had set in and a significant amount of current had built up in the fan-plane, a cut-out of size $44 \times 25 \times 16$ Mm of the MHD state was passed on to a particle-in-cell (PIC) code. With a resolution as high as 17.5 km and a number of particles of up to 136 billion, the underlying particle acceleration mechanism was studied for this pre-flare phase. In order to cover such enormous spatial ranges and at the same time resolving the kinetic scales in the corona, which in reality are just a few mm or cm, the speed of light as well as the charge per particle were modified. Similar modifications have previously been employed by Drake et al. (2006b), who reduced the speed of light or by Siversky and Zharkova (2009), by lowering the particle density.

The results show that the electric current sheets inherited from the MHD simulation on the one hand persist, on average—as they must, in order to match the change in magnetic field line directions across the current sheet. The upper panel of Fig. 10 shows the initial current density in the x–y plane. On the other hand on small scales (similar to ion gyro

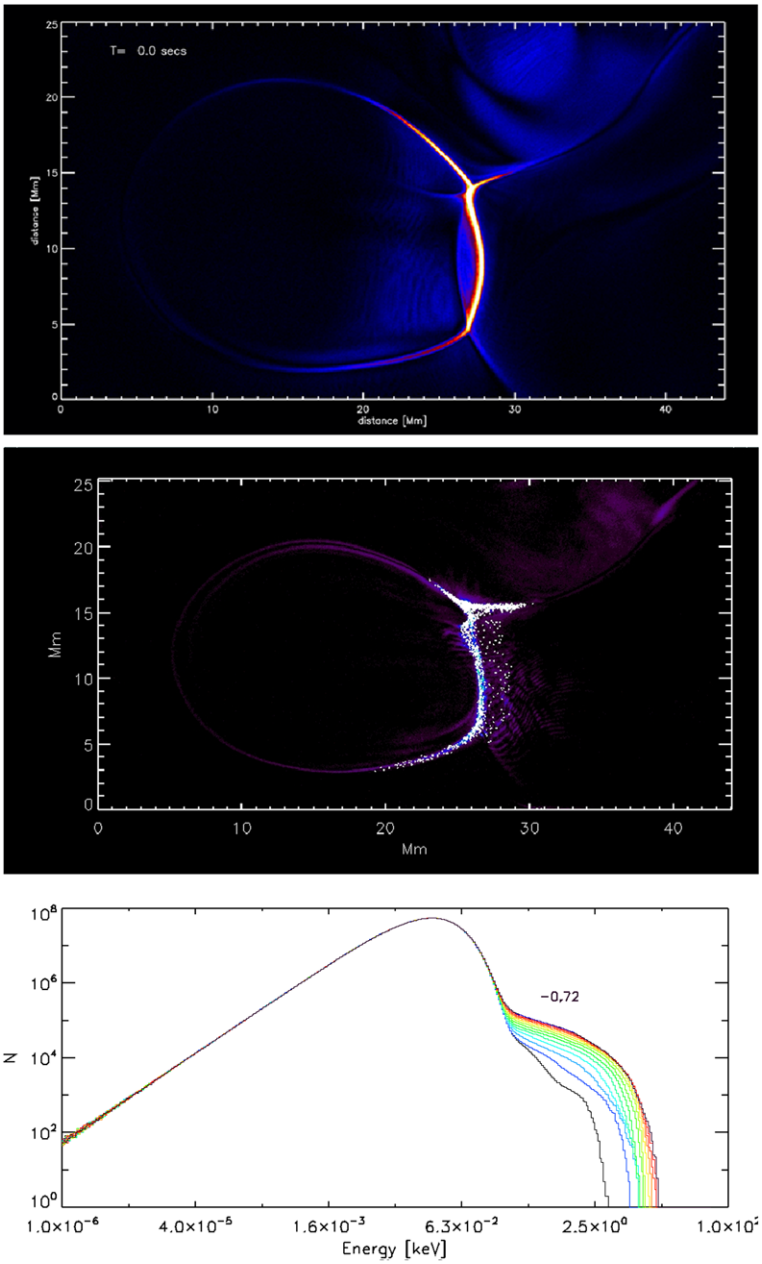

Fig. 10 The *top panel* shows the current in the x–y plane in the PIC simulation described in Sect. 4.5. The *middle panel* shows the position of the higher energy particles during the acceleration by the current sheet electric fields. The *lowest panel* shows the electron distribution function summed over the entire simulation with time increasing in the colored curves from left to right. From Baumann et al. (2012b)

radii), the current sheet breaks up after several seconds and becomes turbulent. In the current sheet there is thus both a systematic "fan-plane" electric field, responsible for supporting the electric current that matches the curl of the magnetic field, and a more turbulent and time varying electric field, generated by chaotic small scale motions.

The systematic electric field gives rise to an impulsive initial electron acceleration, which is represented by a power-law energy distribution in the high energy tail of a Maxwell–Boltzmann distribution. The middle panel of Fig. 10 shows the positions of the high energy-tail particles, which are seen in the vicinity of the current sheet. During the first 1–10 sec, the power-law index rapidly converges toward $\sim dN/dE = -1.77$ for particles moving towards the solar surface in the lower part of the domain, as shown in the lowest panel of Fig. 10. Although they find relatively low particle energies, the DC electric field acceleration mechanism is expected to also be dominant during the much more energetic phase of the flare event. The impact region of the non-thermal electrons in the simulations agrees well with the footpoint emission observations available in several wavelengths. In the lower part of the simulation box, the electron energy of the non-thermal population accounts for more than 50 % of the total energy in this area. Carrying out a similar study, but applying a stratified atmosphere could be used to address the newly proposed model by Brown et al. (2009), as discussed in Sect. 5.

The electric fields available for particle acceleration in both the MHD simulation and the PIC experiment were compared (Baumann et al. 2012b). In both cases they are ultimately a result of the magnetic reconnection taking place in the vicinity of the null-point, which maintains the fan-plane current sheet. Because of the reduction of the electric charge per particle, the parallel electric field in the PIC experiment is several orders of magnitude larger than the resistive electric field in the MHD simulation. In the Sun the corresponding electric field would of course be much smaller. However, even a six orders of magnitude lower electric field would be able to accelerate the small fraction of particles that were in a position to follow the fan-plane along most of their path to energies on the order of 100 keV. This kind of direct electric field acceleration is thus a candidate for explaining the first power law part of the observed electron energy distribution, while acceleration to larger energies could be the result of the fluctuating electric fields also associated with the current sheet.

Clearly such simulations are a long way from modeling an actual flare. That requires much larger computer power capable of reducing the reliance on artificial values of the physical parameters. However it is highly instructive that such a model can, given all the approximations, deliver a power law slope for the accelerated particles that is reasonable.

4.6 An Example of Feedback

Feedback is implicitly present in PIC models, and is now being analyzed for the results of Sect. 4.5 (Baumann et al. 2012b). However, it has also been explored in the 2-D multi current-layer system presented in Sect. 4.1. As we noted there, the Fermi mechanism causes the particle parallel energy to increase and the perpendicular energy to decrease modestly. A strong pressure anisotropy develops within the magnetic islands as particles gain energy, and this continues until the island cores reach the marginal stability condition for the firehose instability. Figure 11 shows the development of pressure anisotropy for the multi current-layer simulation discussed in Sect. 4.1 and Fig. 5. The initial state corresponds to a single point and as particle acceleration proceeds, the parallel pressure increases strongly while the perpendicular pressure has a more modest increase. The upper and lower red lines correspond to the ideal MHD mirror and firehose stability thresholds, respectively.

At late times the plasma bumps against the firehose stability condition even though the initial value of β is very low. This result suggests that even in the low β corona, reconnection

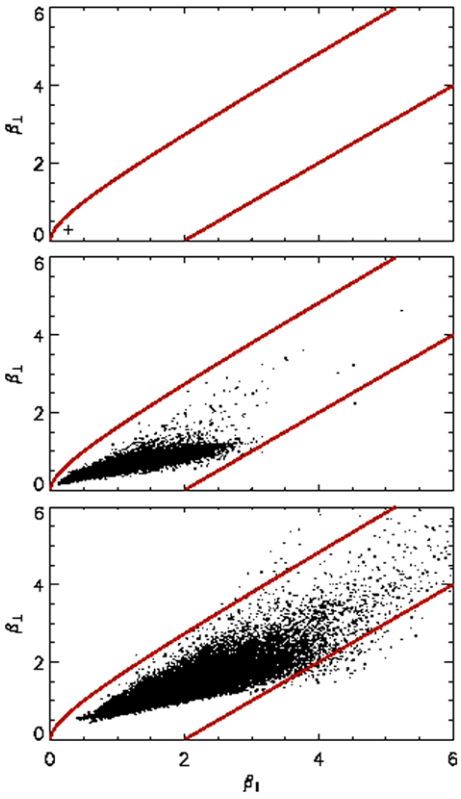

Fig. 11 The values the plasma beta parallel and perpendicular to the local magnetic field at $t = 0$, 100 and 200, from the simulation shown in Figs. 5 and 6 with time in the same dimensionless units. The *upper red curve* is the MHD mirror stability boundary ($\beta_\perp - \beta_{||} = \beta_{||}/\beta_\perp$). The *lower red curve* is the MHD firehose stability boundary ($\beta_{||} - \beta_\perp = 2$)

can drive particle heating and acceleration until the ambient plasma pressure approaches that of the magnetic field. Of course, this requires the free energy that is available in the magnetic field be sufficient to supply the requisite energy. The impact of the approach to the firehose condition in the core of magnetic islands is profound. At the marginal firehose condition the tension in magnetic field goes to zero and therefore the driver for reconnection, which is the relaxation of tension in elongated islands, also goes away. Reconnection is therefore quenched. Thus, the firehose condition becomes an important player in the self-consistent development of reconnection and particle acceleration.

5 Discussion and Conclusions

This paper has outlined how particle acceleration can occur in a coronal magnetic field where (a) individual current sheets break up or fragment and/or (b) the global magnetic field evolves to give a multiplicity of current sheets. The work of the last two decades has demonstrated how such complex electromagnetic fields are the natural state of a driven corona and can account for fundamental properties such as flare energy distributions.

Studying acceleration in such a medium reveals a fascinating picture of how particle acceleration to high energies can occur via multiple interaction with direct electric fields. Indeed in the absence of feedback, such models have an embarrassingly large efficiency, suggesting at first sight that the "number problem" is resolvable. Caution is required since

it is unclear whether feedback simply limits acceleration to the available free energy, as discussed in Sect. 4.6, or has a more drastic effect.

The scenario for flares that we have discussed seems to be at variance with a commonly presented "standard model" alternative (e.g. Shibata and Magara 2011 and references therein). While there is no doubt that mass ejections play a major role in large flares, the "plasmoid-induced reconnection" proposed by Shibata (1998) and many other authors leads inexorably to a single current sheet, and it has never been demonstrated how the required number of electrons can be accelerated in this "standard model". Fragmentation of such a current sheet into smaller structures may offer a more promising way forward, providing not only multiple accelerator sites, but also the presence of meso-scale turbulence to both confine the particles to the vicinity of the accelerators and provide secondary acceleration. But, again, there is no documentation as to how this would work in the context of the standard model. So it seems clear that (a) for smaller, non-eruptive, flares (referred to in the past as compact flares), the eruption-based "standard model" scenario must be treated with skepticism, if not dismissed completely, and (b) for large flares, it is time to consider how distributed accelerators in the entire corona would perform.

It is also unclear if the work presented here can address the coronal "number problem". If indeed all the particles in the corona are accelerated, there are also problems with how charge neutrality is obtained. Traditionally this has involved the invocation of return current systems, but there has never been any evidence that this can work in the global context. Brown et al. (2009) have made an important attempt to circumvent this. They argued that if the acceleration sites were moved to the upper chromosphere/lower transition region, many fewer electrons would be needed to produce the observed HXR flux due to (a) the higher density there and (b) the fact that the electrons can gain and lose energy many times. Brown et al. demonstrated the feasibility of this through test-particle modeling using the Turkmani et al. (2006) model, but with parameters commensurate with the upper chromosphere.

There are though some difficulties. The resolution of the number problem does not change the requirements on the energy released in the flare, since the basic interpretation of the HXR radiation in terms of the electron distribution does not change significantly. This then implies that almost all the free energy released must be tapped from the very narrow region (2000 km wide, say) where the acceleration is taking place. This is not credible in a scenario where the coronal field is stressed slowly, and then relaxes impulsively. If the free energy in the field is confined to the footpoints, it will rapidly spread out as Alfven waves, and the required energy density will be lost rapidly. On the other hand if the whole corona is stressed, why does the small footpoint region decide to become unstable on its own?

One way around these difficulties has been suggested by Fletcher and Hudson (2008) who proposed that coronal magnetic reconnection leads to the propagation of a pair of large-amplitude Alfven waves towards each footpoint. This was discussed in terms of the "standard model" (i.e. a single coronal reconnection site), and MHD simulations of Birn et al. (2009) showed that for a force-free magnetic field, approximately 50 % of the Poynting flux entering the large coronal current sheet exits as a Poynting flux directed towards the footpoints. In a large flare, the amplitude of these waves can be large (several hundred km/s) and perhaps such oscillations would be visible with contemporary instrumentation that makes direct images of transverse wave motion (e.g. McIntosh et al. 2011). The actual acceleration process here is not clear, though Fletcher and Hudson proposed a mode conversion to the kinetic Alfven wave, which in turn can accelerate the particles.

This Fletcher and Hudson scenario implies that coronal acceleration is not efficient, perhaps due to the failure of return currents to replenish the plasma. Yet coronal acceleration of electrons does occur to some degree (Krucker et al. 2008). Finally we note that this energy

transport method is equally applicable in a confined loop with multiple current sheets, as we discussed in Sect. 2.

In summary, there is a need to reconsider old models for flares to take into account new evidence from plasma physics as to how current sheets behave. The essential physics is only beginning to be understood, and furthering such basic studies must be the immediate goal. Only then can any sort of a discussion of detailed flare observations be undertaken.

Acknowledgements We thank many collaborators who have contributed over the years to these ideas. JFD acknowledges support from NSF grant ATM-0903964. G.B. and Å.N. acknowledge support from the SOLAIRE Research Training Network of the European Commission (MRTN-CT-2006-035484). In addition, G.B. acknowledges support from the Niels Bohr International Academy and the John von Neumann Institute for Computing, and Å.N. acknowledges support from PRACE (Partnership for Advanced Computing in Europe) and the European Commission's Seventh Framework Programme (FP7/2007-2013) under the grant agreement SWIFF (project No. 263340, www.swiff.eu).

References

K. Arzner, L. Vlahos, Astrophys. J. Lett. **605**, L69 (2004)
M.J. Aschwanden, B.R. Dennis, A.O. Benz, Astrophys. J. **497**, 972 (1998)
P. Bak, *How Nature Works* (Oxford University Press, Oxford, 1999)
G. Baumann, K. Galsgaard, A. Nordlund, Solar Phys. (2012a, in press). arXiv:1203.1018v1
G. Baumann, T. Haugbolle, A. Nordlund, Astrophys. J. (2012b, in press). arXiv:1204.4947v2
A.O. Benz, Living Rev. Sol. Phys. **5**, 1 (2008)
N.H. Bian, P.K. Browning, Astrophys. J. Lett. **687**, L111 (2008)
J. Birn et al., J. Geophys. Res. **106**, 3715 (2001)
J. Birn, L. Fletcher, M. Hesse, T. Neukirch, Astrophys. J. **695**, 1151 (2009)
J.C. Brown, Sol. Phys. **18**, 489 (1971)
J.C. Brown, R. Turkmani, E.P. Kontar, A.L. MacKinnon, L. Vlahos, Astron. Astrophys. **508**, 993 (2009)
P.K. Browning, C. Gerrard, A.W. Hood, R. Kevis, R.A.M. Van der Linden, Astron. Astrophys. **485**, 837 (2008)
E. Buchlin, M. Velli, Astrophys. J. **662**, 701 (2007)
P.A. Cassak, M.A. Shay, J.F. Drake, Phys. Rev. Lett. **95**, 235002 (2005)
P.J. Cargill, E.R. Priest, Sol. Phys. **76**, 357 (1982)
P.J. Cargill, EOS **77**, 353 (1996)
P.J. Cargill, L. Vlahos, R. Turkmani, K. Galsgaard, H. Isliker, Space Sci. Rev. **124**, 249 (2006)
P. Charbonneau, S.W. McIntosh, H.-L. Liu, T.J. Bogdan, Sol. Phys. **203**, 321 (2001)
J. Chen, J. Geophys. Res. **97**, 15011 (1992)
N.B. Crosby, M.J. Aschwanden, B.R. Dennis, Sol. Phys. **143**, 275 (1993)
S. Dalla, P.K. Browning, Astrophys. J. Lett. **640**, L99 (2006)
W. Daughton, V. Roytershteyn, H. Karimabadi, L. Yin, B.J. Albright, B. Bergen, K.J. Bowers, Nat. Phys. **7**, 539 (2011)
M. Dimitropoulou, M. Georgoulis, H. Isliker, L. Vlahos, A. Anastasiadis, D. Strintzi, X. Moussas, Astron. Astrophys. **505**, 1245 (2009)
M. Dimitropoulou, H. Isliker, L. Vlahos, M. Georgoulis, Astron. Astrophys. **529**, 101 (2011)
J.F. Drake, M. Swisdak, H. Che, M.A. Shay, Nature **443**, 553 (2006a)
J.F. Drake, M. Swisdak, K.M. Schoeffler, B.N. Rogers, S. Kobayashi, Geophys. Res. Lett. **33**, L13105 (2006b)
J.F. Drake, P.A. Cassak, M.A. Shay, M. Swisdak, E. Quataert, Astrophys. J. Lett. **700**, L16 (2009)
J.F. Drake, M. Opher, M. Swisdak, J.N. Chamoun, Astrophys. J. **709**, 963 (2010)
P. Dmitruk, W.H. Matthaeus, N. Seenu, M.R. Brown, Astrophys. J. **597**, L81 (2003)
G. Einaudi, M. Velli, Phys. Plasmas **6**, 4146 (1999)
A.G. Emslie, J.A. Miller, J.C. Brown, Astrophys. J. Lett. **602**, L69 (2004)
L. Fletcher, H.S. Hudson, Astrophys. J. **675**, 1645 (2008)
L. Fletcher, B.R. Dennis, H.S. Hudson, S. Krucker, K. Phillips, A. Veronig, M. Battaglia, L. Bone, A. Caspi, Q. Chen, P. Gallagher, P.T. Grigis, H. Ji, W. Liu, R.O. Milligan, M. Temmer, Space Sci. Rev., **159**, 19 (2011)
K. Galsgaard, A. Nordlund, J. Geophys. Res. **101**, 13445 (1996)

K. Galsgaard, in *SOLMAG 2002, ESA SP-505* (2002)
M. Gordovskyy, P.K. Browning, Astrophys. J. **729**, 101 (2011)
B.V. Gudiksen, A. Nordlund, Astrophys. J. **618**, 1020 (2005)
J. Heyvaerts, E.R. Priest, D.M. Rust, Astrophys. J. **216**, 123 (1977)
A.W. Hood, P.K. Browning, R.A.M. Van der Linden, Astron. Astrophys. **506**, 913 (2009)
A.W. Hood, V. Archontis, D. MacTaggart, Solar Phys. **278**, 3 (2012)
H.S. Hudson, Sol. Phys. **57**, 237 (1978)
P.A. Isenberg, J. Geophys. Res. **91**, 1699 (1986)
H. Isliker, A. Anastasiadis, L. Vlahos, Astron. Astrophys. **377**, 1068 (2001)
H. Karimabadi, W. Daughton, J. Scudder, Geophys. Res. Lett. **34**, L13104 (2007)
M. Kundu, M.N. Gopalswamy, S. White, P. Cargill, E.J. Schmahl, E. Hildner, Astrophys. J. **347**, 505 (1989)
K. Knizhnik, M. Swisdak, J.F. Drake, Astrophys. J. **743**, L35 (2011)
R.A. Kopp, G.W. Pneuman, Sol. Phys. **50**, 85 (1976)
S. Krucker, M. Battaglia, P.J. Cargill, L. Fletcher, H.S. Hudson, A.L. MacKinnon, S. Masuda, L. Sui, M. Tomczak, A.L. Veronig, L. Vlahos, S.M. White, Astron. Astrophys. Rev. **16**, 155 (2008)
S. Krucker, H.S. Hudson, L. Glesener, S.M. White, S. Masuda, J.-P. Wuelser, R.P. Lin, Astrophys. J. **714**, 1108 (2010)
A. Lazarian, this issue (2012)
R.P. Lin, S. Krucker, G.J. Hurford, D.M. Smith, H.S. Hudson, G.D. Holman, R.A. Schwartz, B.R. Dennis, G.H. Share, R.J. Murphy, A.G. Emslie, C. Johns-Krull, N. Vilmer, Astrophys. J. Lett. **595**, L69 (2003)
D.W. Longcope, A.C. Des Jardins, T. Carranza-Fulmer, J. Qiu, J. Sol. Phys. **267**, 107 (2010)
E.T. Lu, R.J. Hamilton, Astrophys. J. Lett. **380**, L89 (1991)
P.C.H. Martens, A. Young, Astrophys. J. Suppl. Ser. **73**, 333 (1988)
S. McIntosh et al., Nature **475**, 477 (2011)
R.C. Maclean, C.E. Parnell, K. Galsgaard, Sol. Phys. **260**, 299 (2009)
J.A. Miller, D.A. Roberts, Astrophys. J. **452**, 912 (1995)
J.A. Miller, T.N. Larosa, R.L. Moore, Astrophys. J. **461**, 445 (1996)
J.A. Miller, P.J. Cargill, A.G. Emslie, G.D. Holman, B.R. Dennis, T.N. LaRosa, R.M. Winglee, S.G. Benka, S. Tsuneta, J. Geophys. Res. **102**, 14631 (1997)
L.I. Miroshnichenko, B. Mendoza, R. Perez-Enriquez, Sol. Phys. **202**, 151 (2001)
A. Nordlund, K. Galsgaard, Astrophys. J. (2012)
M. Oka, T.-D. Phan, S. Krucker, M. Fujimoto, I. Shinohara, Astrophys. J. **714**, 915 (2010)
M. Onofri, H. Isliker, L. Vlahos, Phys. Rev. Lett. **96**, 151102 (2006)
A.V. Oreshina, B.V. Somov, Astron. Astrophys. Trans. **25**(4) 261–273 (2006)
V. Petrosian, this issue (2012). doi:10.1007/s11214-012-9900-6
H.E. Petschek, NASA Spec. Publ. **50**, 425 (1964)
A.F. Rappazzo, M. Velli, G. Einaudi, Astrophys. J. **722**, 65 (2010)
J. Raymond, R.P. Lin, S. Krucker, V. Petrosian, this issue (2012). doi:10.1007/s11214-012-9897-x
K.M. Schoeffler, J.F. Drake, M. Swisdak, Astrophys. J. **743**, 70 (2011)
M.A. Shay, J.F. Drake, M. Swisdak, Phys. Rev. Lett. **99**, 155002 (2007)
K. Shibata, in *Proc. Nobeyama Symp.*, vol. 381 (1998), NRO report 479
K. Shibata, T. Magara, Living Reviews. Sol. Phys. **8**, 6 (2011)
A.Y. Shih, R.P. Lin, D.M. Smith, Astrophys. J. **698**, L152 (2009)
T.V. Siversky, V.V. Zharkova, J. Plasma Phys. **75**, 619 (2009)
T.W. Speiser, J. Geophys. Res. **70**, 4129 (1965)
P.A. Sturrock, Nature **211**, 695 (1966)
R. Turkmani, L. Vlahos, K. Galsgaard, P.J. Cargill, H. Isliker, Astrophys. J. Lett. **620**, L59 (2005)
R. Turkmani, P.J. Cargill, K. Galsgaard, L. Vlahos, H. Isliker, Astron. Astrophys. **449**, 749 (2006)
D. Vassiliadis, A. Anastasiadis, M. Georgoulis, L. Vlahos, Astrophys. J. Lett. **509**, L53 (1998)
L. Vlahos, M. Georgoulis, R. Kluiving, P. Paschos, Astron. Astrophys. **299**, 897 (1995)
L. Vlahos, M. Georgoulis, Astrophys. J. Lett. **603**, L61 (2004a)
L. Vlahos, H. Isliker, F. Lepreti, Astrophys. J. **608**, 540 (2004b)
L. Vlahos, S. Krucker, P.J. Cargill, in *Turbulence in Space Plasmas*, ed. by L. Vlahos, P.J. Cargill (Springer, Berlin, 2009)